Hybrid-Mode Analysis of Coupled Microstrip-Slot Resonators

KENJI KAWANO

Abstract—**An advanced microwave and millimeter-wave integrated circuit element, that is, a coupled microstrip resonator with a tuning slot, or a coupled microstrip-slot resonator, has been developed. As special cases, a microstrip-slot resonator, coupled microstrip resonator, and microstrip resonator have been investigated.**

A hybrid-mode analysis is presented for obtaining resonant frequencies. It is based upon Galerkin's method in the Forier transform domain. The Green functions in this domain, which are versatile and applicable to other microstrip-slot structures, are shown in simple form.

Computed resonant frequencies and measured resonant values are compared for aluminum substrates in the 3–7-GHz frequency range.

I. Introduction

MICROSTRIP resonators are indispensable circuit elements for microwave and millimeter-wave integrated circuits [1]. They have been analyzed by many authors [2]–[5]. After microstrip resonators were analyzed by Itoh [6], who used a hybrid-mode analysis in the Fourier transform domain, the spectral-domain approach has been used to successively solve various resonant structures [7]–[9]. Furthermore, Chew and Kong investigated resonant frequencies of microstrip disk resonators through the spectral-domain approach and perturbation theory [10].

Meanwhile, Aikawa has developed coupled microstrip lines with tuning septums, which are useful for realization of a tightly coupled directional coupler [11]. These structures, which include microstrip lines with tuning septums, have been analyzed through the spectral-domain approach [12]–[14].

However, to the best knowledge of the author, these structures have not been introduced into resonators, although they have been thought useful. To date, microstrips and slots are located on only one surface of the substrate.

In this paper, a coupled microstrip resonator with a tuning slot, namely, a coupled microstrip-slot resonator, is presented as a circuit element for microwave and millimeter-wave integrated circuits. Such a structure is shown in Fig. 1. This resonator has microstrips and a slot on each side of the substrate. Furthermore, a hybrid-mode analysis is presented for obtaining the resonant frequencies of this resonator. It is based upon Galerkin's method in the Fourier transform domain.

Manuscript received August 8, 1983; revised July 8, 1984.

The author is with the Musashino Electrical Communication Laboratory, Nippon Telegraph and Telephone Public Corporation, 3-9-11, Midoricho, Musashino-shi, Tokyo 180, Japan.

As special cases, a microstrip-slot resonator, coupled microstrip resonator, and microstrip resonator are also investigated.

In Section II, the formulation process is described and Green functions are derived. In Section III, computed resonant frequencies are compared with measured values for alumina substrates. Although the number of the basis functions is small and functional forms are simple, it is shown that both results agree relatively well.

II. Analytical Method

The hybrid-mode analysis based on Galerkin's method in the spectral domain is already conventional. As the detailed analytical procedure is discussed in [6] and [15], only a brief description will be given in this section. The various analyzed microstrip-slot structures are shown in Figs. 1 and 2. Fig. 1 shows a coupled microstrip-slot resonator in which two microstrips of width $2W_R$, length $2X_R$, and separation $2S_R$, as well as a slot of width $2W_L$ and length $2X_L$, are located on each side of a substrate of thickness D. Fig. 2 shows a microstrip-slot resonator. It was assumed that metals are infinitely thin and perfect conductors, and the substrate material, whose permittivity and permeability are ϵ_r and μ_r, respectively, is lossless. It was also assumed for simplicity that the structure is symmetric with respect to the y-axis.

The electromagnetic fields in the spectral domain are expressed by the Fourier transformed scalar potentials. For instance

$$\tilde{E}zi(n, y, \beta) = (k_i^2 - \beta^2)\tilde{\psi}_i^e(n, y, \beta) \quad (1a)$$

$$\tilde{H}zi(n, y, \beta) = (k_i^2 - \beta^2)\tilde{\psi}_i^h(n, y, \beta) \quad (1b)$$

where subscript i designates each region defined as 1, 2, and 3 in Figs. 1 and 2, and where

$$k_i^2 = \omega^2 \epsilon_i \mu_i \quad (2)$$

where ω is the angular resonant frequency, and ϵ_i and μ_i are the permittivity and permeability in region i, respectively. β is the Fourier transform variable. $\tilde{\psi}^e(n, y, \beta)$ and $\tilde{\psi}^h(n, y, \beta)$ are the Fourier transformed electric and magnetic scalar potentials, respectively. Here, the Fourier transformation is defined as follows:

$$\tilde{f}(n, y, \beta) = \int_{-\infty}^{\infty} dz \int_{-A}^{A} dx f(x, y, z) e^{j(k_n x + \beta z)} \quad (3)$$

0018-9480/85/0100-0038$01.00 ©1984 IEEE

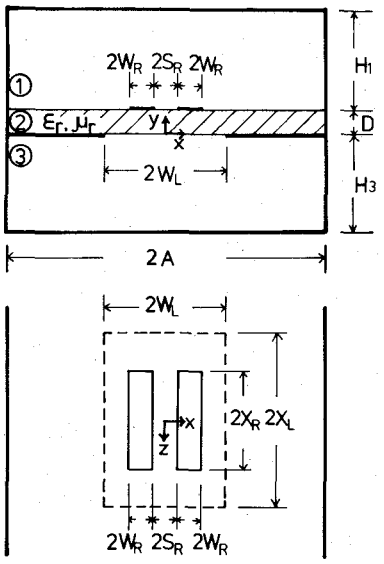

Fig. 1. Conceptualized external view of coupled microstrip-slot resonator and coordinate system.

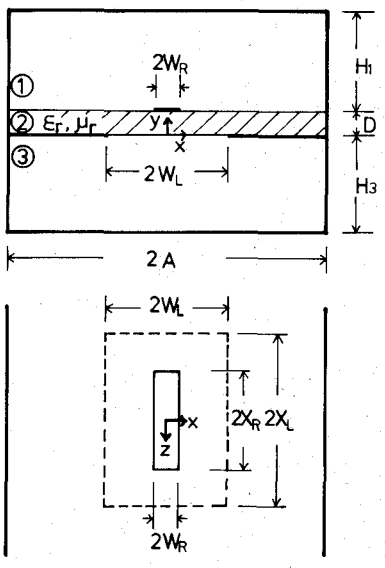

Fig. 2. Conceptualized external view of microstrip-slot resonator and coordinate system.

where

$$k_n = \begin{cases} \dfrac{(n-0.5)\pi}{A}, & \text{for } Hz \text{ odd mode in } x \\ \dfrac{n\pi}{A}, & \text{for } Hz \text{ even mode in } x. \end{cases} \tag{4}$$

Applying the boundary conditions at shielding walls, the Fourier transformed scalar potentials in (1) are derived from the transformed Helmholtz equation. By substituting the transformed fields, which include the scalar potentials in the spectral domain, into the transformed boundary conditions at interfaces at $y = D$ and 0, the following matrix equation, which relates the electric field and current density components, can be derived:

$$\begin{pmatrix} \tilde{G}_{11}(n,\omega,\beta) & \tilde{G}_{12}(n,\omega,\beta) & \tilde{G}_{13}(n,\omega,\beta) & \tilde{G}_{14}(n,\omega,\beta) \\ \tilde{G}_{21}(n,\omega,\beta) & \tilde{G}_{22}(n,\omega,\beta) & \tilde{G}_{23}(n,\omega,\beta) & \tilde{G}_{24}(n,\omega,\beta) \\ \tilde{G}_{31}(n,\omega,\beta) & \tilde{G}_{32}(n,\omega,\beta) & \tilde{G}_{33}(n,\omega,\beta) & \tilde{G}_{34}(n,\omega,\beta) \\ \tilde{G}_{41}(n,\omega,\beta) & \tilde{G}_{42}(n,\omega,\beta) & \tilde{G}_{43}(n,\omega,\beta) & \tilde{G}_{44}(n,\omega,\beta) \end{pmatrix} \cdot \begin{pmatrix} \tilde{J}_x(n,\beta) \\ \tilde{J}_z(n,\beta) \\ \tilde{E}_x(n,\beta) \\ \tilde{E}_z(n,\beta) \end{pmatrix} = \begin{pmatrix} \tilde{e}_z(n,\beta) \\ \tilde{e}_x(n,\beta) \\ \tilde{I}_x(n,\beta) \\ \tilde{I}_z(n,\beta) \end{pmatrix} \tag{5}$$

where $\tilde{G}_{11}, \cdots, \tilde{G}_{44}$ are the dyadic Green functions in the Fourier transform domain. $\tilde{J}_x(n,\beta)$, $\tilde{J}_z(n,\beta)$, $\tilde{e}_x(n,\beta)$, and $\tilde{e}_z(n,\beta)$ are the Fourier transformed currents and fields at $y = D$. $\tilde{I}_x(n,\beta)$, $\tilde{I}_z(n,\beta)$, $\tilde{E}_x(n,\beta)$, and $\tilde{E}_z(n,\beta)$ are the same parameters at $y = 0$. For instance

$$\tilde{J}_q(n,\beta) = \int_{-X_R}^{X_R} dz \int_{-W_R}^{W_R} dx J_q(x,z) e^{j(k_n x + \beta z)} \tag{6}$$

where $q = x$ and z, and $J_q(x,z)$ is the strip current density functions in the space domain.

Although the Green functions can be computed without mathematical manipulation [16], [17], they have been analytically obtained in order to reduce computer time. Their expressions are shown in the Appendix in simple form. It is to be noted that $\tilde{G}_{11}$, $\tilde{G}_{12}$, $\tilde{G}_{21}$, and $\tilde{G}_{22}$ are related to the strip currents, and $\tilde{G}_{33}$, $\tilde{G}_{34}$, $\tilde{G}_{43}$, and $\tilde{G}_{44}$ are related to the slot fields. Other Green functions represent the interactions between the strip currents and slot fields. As these Green functions are not explicit functions of resonator geometry, they are versatile and applicable to various microstrip-slot structures. Although, up to this point, the formulation has been exact, some approximation is now necessary to solve (5).

To this end, Galerkin's method in the Fourier transform domain has been chosen, which enables us to eliminate the unknown electric field and current density functions, $\tilde{e}_q(n,\beta)$ and $\tilde{I}_q(n,\beta)$. Let us expand the unknown strip current density functions $\tilde{J}_q(n,\beta)$ and slot field functions $\tilde{E}_q(n,\beta)$ in terms of known basis functions $\tilde{J}_{qm}(n,\beta)$ and $\tilde{E}_{qm}(n,\beta)$, respectively.

A. Top Substrate Surface ($y = D$)

$$\tilde{J}_x(n,\beta) = \sum_{m=1}^{K} a_m \tilde{J}_{xm}(n,\beta) \tag{7a}$$

$$\tilde{J}_z(n,\beta) = \sum_{m=1}^{L} b_m \tilde{J}_{zm}(n,\beta). \tag{7b}$$

B. Bottom Substrate Surface ($y = 0$)

$$\tilde{E}_x(n,\beta) = \sum_{m=1}^{M} c_m \tilde{E}_{xm}(n,\beta) \tag{8a}$$

$$\tilde{E}_z(n,\beta) = \sum_{m=1}^{N} d_m \tilde{E}_{z_m}(n,\beta) \tag{8b}$$

where a_m, b_m, c_m, and d_m are unknown expansion coefficients.

Substituting (7) and (8) into (5), and taking inner products with $\tilde{J}_{zl}(n,\beta)$, $\tilde{J}_{xi}(n,\beta)$, $\tilde{E}_{xi}(n,\beta)$, and $\tilde{E}_{zl}(n,\beta)$, respectively, a set of $(K+L)\times(M+N)$ simultaneous equations with $(K+L)\times(M+N)$ unknown expansion coefficients can be obtained

$$\sum_{m=1}^{K} D_{im}^{11}(\omega)a_m + \sum_{m=1}^{L} D_{im}^{12}(\omega)b_m + \sum_{m=1}^{M} D_{im}^{13}(\omega)C_m + \sum_{m=1}^{N} D_{im}^{14}(\omega)\,d_m = 0 \qquad i=1,2,\cdots,L \quad (9a)$$

$$\sum_{m=1}^{K} D_{im}^{21}(\omega)a_m + \sum_{m=1}^{L} D_{im}^{22}(\omega)b_m + \sum_{m=1}^{M} D_{im}^{23}(\omega)C_m + \sum_{m=1}^{N} D_{im}^{24}(\omega)\,d_m = 0 \qquad i=1,2,\cdots,K \quad (9b)$$

$$\sum_{m=1}^{K} D_{im}^{31}(\omega)a_m + \sum_{m=1}^{L} D_{im}^{32}(\omega)b_m + \sum_{m=1}^{M} D_{im}^{33}(\omega)C_m + \sum_{m=1}^{N} D_{im}^{34}(\omega)\,d_m = 0 \qquad i=1,2,\cdots,M \quad (9c)$$

$$\sum_{m=1}^{K} D_{im}^{41}(\omega)a_m + \sum_{m=1}^{L} D_{im}^{42}(\omega)b_m + \sum_{m=1}^{M} D_{im}^{43}(\omega)C_m + \sum_{m=1}^{N} D^{44}(\omega)\,d_m = 0 \qquad i=1,2,\cdots,N \quad (9d)$$

where one typical matrix element is given by

$$D_{im}^{12}(\omega) = \sum_{n=-\infty}^{\infty} \int_{-\infty}^{\infty} d\beta \tilde{J}_{zi}(n,\beta)\tilde{G}_{12}(n,\omega,\beta)\tilde{J}_{zm}(n,\beta). \quad (10)$$

The right-hand side of (9) has been derived by virtue of Parseval's theorem, since the strip currents and electric fields are zero in the complementary regions at interfaces $y=D$ and $y=0$. The characteristic equation for the angular resonant frequency can be obtained from (9) by setting the determinant of the coefficient matrix $D(\omega)$ equal to zero

$$|D(\omega)| = 0. \quad (11)$$

If the basis functions $\tilde{J}_{qm}(n,\beta)$ and $\tilde{E}_{qm}(n,\beta)$ are chosen such that their inverse Fourier transforms resemble the actual unknown strip current density and slot field components, good results can be obtained using only a few basis functions [6], [18], [19]. This makes the matrix size of (11) small, resulting in a necessity for less computer time. It was also desirable that $\tilde{J}_{qm}(n,\beta)$ and $\tilde{E}_{qm}(n,\beta)$ can be analytically obtained, so as to reduce computer time. As the assumption $J_x(x,z)=0$ gives good results for a narrow microstrip resonator [6], we set K equal to zero for the coupled microstrip-slot resonator. Furthermore, only one basis function has been chosen for each $E_x(x,z)$ and $E_z(x,z)$, respectively. This means $L=M=N=1$. Therefore, their inverse transforms are

$$J_{z1}(x,z) = J_1(x)\cdot J_2(z) \quad (12a)$$

$$E_{x1}(x,z) = E_1(x)\cdot E_2(z) \quad (12b)$$

$$E_{z1}(x,z) = E_3(x)\cdot E_4(z). \quad (12c)$$

The remaining problem is to determine functional forms. For $J_1(x)$ and $J_2(z)$, the following functions [6] are assumed for the even-mode resonance of coupled microstrip-slot resonator:

$$J_1(x) = \begin{cases} \left(1+\left|\dfrac{x\pm(S_R+W_R)}{W_R}\right|^3\right), & S_R<|x|<S_R+2W_R \\ 0, & \text{elsewhere} \end{cases} \quad (13a)$$

$$J_2(z) = \begin{cases} \cos\dfrac{\pi z}{2x_R}, & |z|<X_R \\ 0, & \text{elsewhere} \end{cases} \quad (13b)$$

For the odd-mode resonance, (13a) should be changed antisymmetrically.

As far as the slot fields are concerned, the following simple basis functions have been chosen for the microstrip-slot resonator and even-mode resonance of the coupled microstrip-slot resonator:

$$E_1(x) = \begin{cases} 1, & 0<x<W_L \\ -1, & -W_L<x<0 \\ 0, & \text{elsewhere} \end{cases} \quad (14a)$$

$$E_2(z) = \begin{cases} \cos\dfrac{\pi z}{2X_L}, & |z|<X_L \\ 0, & \text{elsewhere} \end{cases} \quad (14b)$$

$$E_3(x) = \begin{cases} 1, & |x|<W_L \\ 0, & \text{elsewhere} \end{cases} \quad (14c)$$

$$E_4(z) = \begin{cases} z, & |z|<X_L \\ 0, & \text{elsewhere.} \end{cases} \quad (14d)$$

Meanwhile, for the odd-mode resonance, the following basis functions have been chosen:

$$E_1(x) = (14c) \quad (15a)$$

$$E_2(z) = (14b) \quad (15b)$$

$$E_3(x) = (14a) \quad (15c)$$

$$E_4(z) = (14d). \quad (15d)$$

The resulting characteristic equation to be solved is a three-dimensional determinant, as follows:

$$\begin{vmatrix} D_{11}^{12}(\omega) & D_{11}^{13}(\omega) & D_{11}^{14}(\omega) \\ D_{11}^{32}(\omega) & D_{11}^{33}(\omega) & D_{11}^{34}(\omega) \\ D_{11}^{42}(\omega) & D_{11}^{43}(\omega) & D_{11}^{44}(\omega) \end{vmatrix} = 0. \quad (16)$$

Now, the boundary value problem is reduced to the numerical seeking for the values of ω. The method of successive bisection [20] has been utilized.

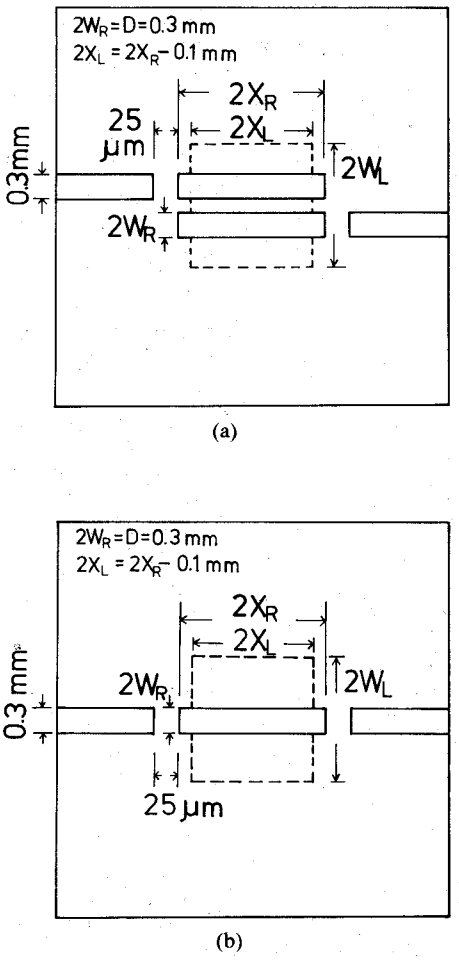

Fig. 3. Experimental geometries for (a) coupled microstrip-slot resonator, and (b) microstrip-slot resonator.

III. Numerical and Experimental Results

Experimental geometries for the coupled microstrip-slot resonator and microstrip-slot resonator are shown in Fig. 3(a) and (b). Microstrips, including input and output terminals for electromagnetic power, as well as tuning slots, are shown as solid lines and dotted lines, respectively.

The coupling gap between the resonator and terminal strips was about 25 μm. An alumina substrate $25 \times 25 \times 0.3$ mm with a relative dielectric constant of 9.6 has been chosen. The metals were 0.02-μm-thick nickel-chromium and 4-μm-thick gold. As the experiments were made in the open, the computation was performed in regard to the large shielding walls, with $2A = 30 \cdot D$ and $H_1 = H_3 = 10 \cdot D$, in order to avoid the effects of the side, upper, and lower ground planes.

Fig. 4 shows computed and measured resonant frequencies for the microstrip-slot resonator, versus microstrip length $2X_R$. Although simple basis functions are used, the agreement between the numerical and experimental results is relatively good. As seen in this figure, resonant frequencies increase as slot width becomes large, which means that the quantity of electromagnetic-field leakage into the lower air region increases with slot width.

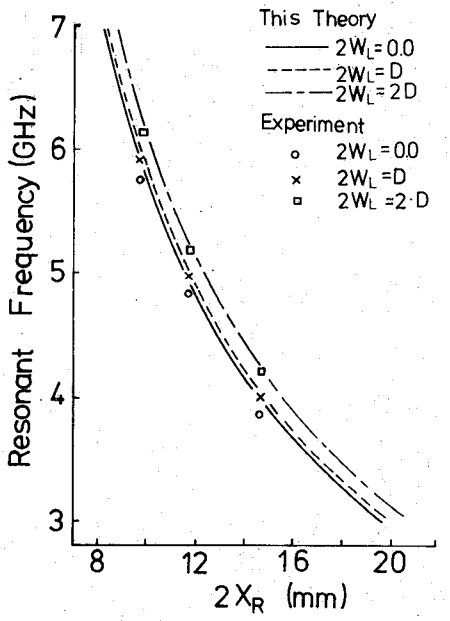

Fig. 4. Computed and measured resonant frequencies for microstrip-slot resonator on alumina substrates versus microstrip length $2X_R$. $\epsilon_r = 9.6$, $2W_R = D = 0.3$ mm. $H_1 = H_3 = 10\ D$, $2A = 30\ D$, and $2X_L = 2X_R - 0.1$ mm.

Fig. 5(a) and (b) shows computed and measured resonant frequencies for the even- and odd-mode resonances of the coupled microstrip-slot resonator versus coupled microstrip length $2X_R$. Similar to the case of the microstrip-slot resonator, it is found that the numerical and experimental results agree relatively well. These figures show that the resonant frequencies are, respectively, strongly and weakly affected by the tuning slot for the even- and odd-mode resonances.

The difference in the behavior of the resonant frequencies between the even- and odd-mode resonances implies the following meanings. For the even mode, there is strong interaction between the strips and a tuning slot. For the odd mode, however, interaction between the two strips becomes strong. As a result, slot width affects the even mode more strongly than the odd mode.

V. Conclusions

The resonant frequencies of a coupled microstrip resonator with a tuning slot, or a coupled microstrip-slot resonator, have been investigated. Furthermore, a numerical method has been presented for obtaining resonant frequencies of a coupled microstrip-slot resonator. It was based upon a hybrid-mode analysis, where Galerkin's method in the Fourier transform domain was used. The dyadic Green functions, which are versatile and applicable to various microstrip-slot structures, were analytically derived to reduce computer time, and have been shown in simple form.

In regard to the microstrip-slot resonator and even-mode resonance of the coupled microstrip-slot resonator, the tuning slot can increase considerably the resonant frequencies. Meanwhile, in relation to the odd-mode resonance, the effect of the slot is small.

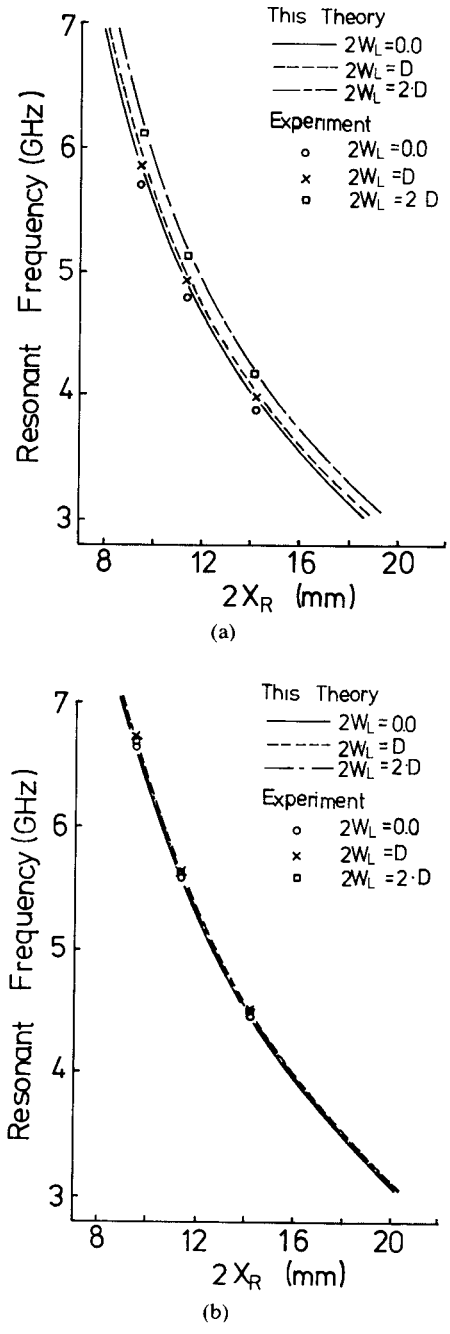

Fig. 5. Computed and measured resonant frequencies for (a) even-mode resonance, and (b) odd-mode resonance of coupled microstrip-slot resonator on alumina substrates versus microstrip length $2X_R$. $\epsilon_r = 9.6$, $2W_R = D = 0.3$ mm, $2S_R = 0.06$ mm. $H_1 = H_3 = 10\ D$, $2A = 30\ D$, and $2X_L = 2X_R - 0.1$ mm.

Acknowledgment

The author would like to acknowledge the continuing guidance and encouragement of H. Sato, J. Kato, and K. Sawamoto. He wishes to express his gratitude to H. Jumonji for observations and a critical reading of the manuscript, and K. Onuki for his helpful discussions. The author deeply appreciates the stimulating suggestions and discussions of M. Aikawa. Thanks are also due to H. Tomimuro and Y. Shimoda for useful discussions.

Appendix

In the following expressions, subscripts 1, 2, and 3 for i designate regions 1, 2, and 3 in Figs. 1 and 2, while $k_i^2 = \omega^2 \epsilon_i \mu_i$ and $\gamma_i^2 = k_n^2 + \beta^2 - k_i^2$

$$\tilde{G}_{11}(n,\omega,\beta) = \frac{j\sinh(\gamma_1 H_1)}{\omega\epsilon_1 \cdot \det} \cdot g_1$$

$$\tilde{G}_{12}(n,\omega,\beta) = \frac{j\sinh(\gamma_1 H_1)}{\omega\epsilon_1 \cdot \det} \cdot g_2$$

$$\tilde{G}_{13}(n,\omega,\beta) = \frac{\sinh(\gamma_1 H_1)}{k_1^2 \cdot \det} \cdot g_3$$

$$\tilde{G}_{14}(n,\omega,\beta) = \frac{\sinh(\gamma_1 H_1)}{k_1^2 \cdot \det} \cdot g_4$$

$$\tilde{G}_{21}(n,\omega,\beta) = \frac{j \cdot \sinh(\gamma_1 H_1)}{\omega\epsilon_1 \cdot \det} \cdot g_5$$

$$\tilde{G}_{22}(n,\omega,\beta) = -\tilde{G}_{11}(n,\omega,\beta)$$

$$\tilde{G}_{23}(n,\omega,\beta) = \frac{\sinh(\gamma_1 H_1)}{k_1^2 \cdot \det} \cdot g_6$$

$$\tilde{G}_{24}(n,\omega,\beta) = \tilde{G}_{13}(n,\omega,\beta)$$

$$\tilde{G}_{31}(n,\omega,\beta) = \tilde{G}_{23}(n,\omega,\beta)$$

$$\tilde{G}_{32}(n,\omega,\beta) = -\tilde{G}_{13}(n,\omega,\beta)$$

$$\tilde{G}_{33}(n,\omega,\beta) = \frac{j}{\omega\mu_2\gamma_1\gamma_2 \cdot \det} \cdot \left\{ g_7 + g_8 \cdot \tanh(\gamma_2 D) + \frac{g_9}{\sinh(\gamma_2 D)\cosh(\gamma_2 D)} \right\}$$

$$\tilde{G}_{34}(n,\omega,\beta) = \frac{j}{\omega\mu_2\gamma_1\gamma_2 \cdot \det} \cdot \left\{ g_{10} + g_{11}\tanh(\gamma_2 D) + \frac{g_{12}}{\sinh(\gamma_2 D)\cosh(\gamma_2 D)} \right\}$$

$$\tilde{G}_{41}(n,\omega,\beta) = -\tilde{G}_{13}(n,\omega,\beta)$$

$$\tilde{G}_{42}(n,\omega,\beta) = \tilde{G}_{14}(n,\omega,\beta)$$

$$\tilde{G}_{43}(n,\omega,\beta) = -\tilde{G}_{34}(n,\omega,\beta)$$

$$\tilde{G}_{44}(n,\omega,\beta) = \frac{-j}{\omega\mu_2\gamma_1\gamma_2 \cdot \det} \cdot \left\{ g_{13} + g_{14}\tanh(\gamma_2 D) + \frac{g_{15}}{\sinh(\gamma_2 D)\cosh(\gamma_2 D)} \right\}$$

$$\det = \{\gamma_2 \cdot \coth(\gamma_1 H_1) \cdot \tanh(\gamma_2 D) + \epsilon_r \gamma_1\} \cdot \{\gamma_2 \cdot \tanh(\gamma_1 H_1) \cdot \coth(\gamma_2 D) + \mu_r \gamma_1\}$$

$$g_1 = k_n \beta \{\mu_r \gamma_2 \cdot \tanh(\gamma_2 D)/\sinh(\gamma_1 H_1) + \gamma_1/\cosh(\gamma_1 H_1)\}$$

$$g_2 = \mu_r \gamma_2 (k_1^2 - \beta^2)\tanh(\gamma_2 D)/\sinh(\gamma_1 H_1) + \gamma_1 (k_2^2 - \beta^2)/\cosh(\gamma_1 H_1)$$

$$g_3 = -k_n \beta (k_1^2 - k_2^2)/\{\sinh(\gamma_1 H_1) \cdot \cosh(\gamma_2 D)\}$$

$$\det = \{\gamma_2 \cdot \coth(\gamma_1 H_1) \cdot \tanh(\gamma_2 D) + \epsilon_r \gamma_1\} \cdot \{\gamma_2 \cdot \tanh(\gamma_1 H_1) \cdot \coth(\gamma_2 D) + \mu_r \gamma_1\}$$

$$g_4 = \epsilon_r \gamma_1 \gamma_2 k_1^2 / \{\cosh(\gamma_1 H_1) \sinh(\gamma_2 D)\} + (k_1^2 k_n^2 + k_2^2 \beta^2 - k_1^2 k_2^2) / \{\sinh(\gamma_1 H_1) \cosh(\gamma_2 D)\}$$

$$g_5 = \mu_r \gamma_2 (k_1^2 - k_n^2) \tanh(\gamma_2 D) / \sinh(\gamma_1 H_1) + \gamma_1 (k_2^2 - k_n^2) / \cosh(\gamma_1 H_1)$$

$$g_6 = (k_1^2 \beta^2 + k_2^2 k_n^2 - k_1^2 k_2^2) / \{\sinh(\gamma_1 H_1) \cdot \cosh(\gamma_2 D)\}$$

$$g_7 = \gamma_2 [\mu_r (k_1^2 - \beta^2)(\epsilon_r \mu_r \gamma_1^2 + \gamma_2^2) \coth(\gamma_3 H_3) + \gamma_1^2 (k_2^2 - \beta^2) \{\epsilon_r \tanh(\gamma_1 H_1) + \mu_r \coth(\gamma_1 H_1)\}]$$

$$g_8 = \gamma_1 [\mu_r \gamma_2^2 (k_1^2 - \beta^2) \{\epsilon_r \tanh(\gamma_1 H_1) + \mu_r \coth(\gamma_1 H_1)\} \cdot \coth(\gamma_3 H_3) + (k_2^2 - \beta^2)(\epsilon_r \mu_r \gamma_1^2 + \gamma_2^2)]$$

$$g_9 = (k_1^2 - \beta^2) \gamma_1 \gamma_2^2 \epsilon_r \mu_r \{\tanh(\gamma_1 H_1) \coth(\gamma_3 H_3) + 1\}$$

$$g_{10} = k_n \beta \gamma_2 [\mu_r (\epsilon_r \mu_r \gamma_1^2 + \gamma_2^2) \coth(\gamma_3 H_3) + \gamma_1^2 \{\epsilon_r \tanh(\gamma_1 H_1) + \mu_r \coth(\gamma_1 H_1)\}]$$

$$g_{11} = k_n \beta \gamma_1 [\mu_r \gamma_2^2 \{\epsilon_r \tanh(\gamma_1 H_1) + \mu_r \coth(\gamma_1 H_1)\} \cdot \coth(\gamma_3 H_3) + (\epsilon_r \mu_r \gamma_1^2 + \gamma_2^2)]$$

$$g_{12} = k_n \beta \gamma_1 \gamma_2^2 \epsilon_r \mu_r \{\tanh(\gamma_1 H_1) \coth(\gamma_3 H_3) + 1\}$$

$$g_{13} = \gamma_2 [\mu_r (k_1^2 - k_n^2)(\epsilon_r \mu_r \gamma_1^2 + \gamma_2^2) \coth(\gamma_3 H_3) + \gamma_1^2 (k_2^2 - k_n^2) \{\epsilon_r \tanh(\gamma_1 H_1) + \mu_r \coth(\gamma_1 H_1)\}]$$

$$g_{14} = \gamma_1 [\mu_r \gamma_2^2 (k_1^2 - k_n^2) \{\epsilon_r \tanh(\gamma_1 H_1) + \mu_r \coth(\gamma_1 H_1)\} \cdot \coth(\gamma_3 H_3) + (k_2^2 - k_n^2)(\epsilon_r \mu_r \gamma_1^2 + \gamma_2^2)]$$

$$g_{15} = (k_1^2 - k_n^2) \gamma_1 \gamma_2^2 \epsilon_r \mu_r \{\tanh(\gamma_1 H_1) \coth(\gamma_3 H_3) + 1\}.$$

REFERENCES

[1] S. Mao, S. Jones, and G. D. Vendelin, "Millimeter-wave integrated circuits," *IEEE Trans. Microwave Theory Tech.*, vol. MTT-16, pp. 455–461, July 1968.

[2] T. Itoh and R. Mittra, "A new method for calculating the capacitance of a circular disk for microwave integrated circuits," *IEEE Trans. Microwave Theory Tech.*, vol. MTT-21, pp. 431–432, June 1973.

[3] T. Itoh, "A method for analyzing the characteristics of some lumped elements in microwave integrated circuits," *Electron. Commun.*, vol. 56-B, no. 8, pp. 339–344, Aug. 1973.

[4] Y. Rahmat-Samii, T. Itoh, and R. Mittra, "A spectral domain analysis for solving microstrip discontinuity problems," *IEEE Trans. Microwave Theory Tech.*, vol. MTT-22, pp. 372–378, Apr. 1974.

[5] I. Wolff and N. Knoppik, "Rectangular and circular microstrip disk capacitors and resonators," *IEEE Trans. Microwave Theory Tech.*, vol. MTT-22, pp. 857–864, Oct. 1974.

[6] T. Itoh, "Analysis of microstrip resonators," *IEEE Trans. Microwave Theory Tech.*, vol. MTT-22, pp. 946–952, Nov. 1974.

[7] T. Itoh and W. Menzel, "A full-wave analysis method for open microstrip structures," *IEEE Trans. Antennas Propagat.*, vol. AP-29, pp. 63–68, Jan. 1981.

[8] J. B. Knorr, "Equivalent reactance of a shorting septum in a fin-line: theory and experiment," *IEEE Trans. Microwave Theory Tech.*, vol. MTT-29, pp. 1196–1202, Nov. 1981.

[9] K. Kawano and H. Tomimuro, "Spectral domain analysis of slot resonator," *Electron. Commun.*, vol. E 65, no. 8, pp. 480–484, Aug. 1982.

[10] W. C. Chew and J. A. Kong, "Resonance of nonaxial symmetric modes in circular microstrip disk antenna," *J. Math. Phys.*, vol. 21, pp. 2590–2598, Oct. 1980.

[11] M. Aikawa, "Microstrip line directional coupler with tight coupling and high directivity," *Electron. Commun.*, vol. J60-B, no. 4, pp. 253–259, Apr. 1977.

[12] T. Itoh and A. S. Herbert, "A generalized spectral domain analysis for coupled suspended microstriplines with tuning septums," *IEEE Trans. Microwave Theory Tech.*, vol. MTT-26, pp. 820–826, Oct. 1978.

[13] R. H. Jansen, "Microstrip lines with partially removed ground metallization, theory and applications," *Arch. Elek. Übertragung.*, vol. 32, pp. 485–492, 1978.

[14] T. Itoh, "Spectral domain immitance approach for dispersion characteristics of generalized printed transmission lines," *IEEE Trans. Microwave Theory Tech.*, vol. MTT-28, pp. 733–736, July 1980.

[15] L. P. Schmidt and T. Itoh, "Spectral domain analysis of dominant and higher order modes in fin-lines," *IEEE Trans. Microwave Theory Tech.*, vol. MTT-28, pp. 981–985, Sept. 1980.

[16] M. Aikawa and H. Ogawa, "Analysis of coupled slots and its application to MIC magic-T," *Tech. Group Electronics and Communication in Japan*, MW78-30, pp. 9–16, June 1980.

[17] J. B. Knorr, "Millimeter-wave fin-line characteristics," *IEEE Trans. Microwave Theory Tech.*, vol. MTT-28, pp. 737–743, July 1980.

[18] K. Kawano and H. Tomimuro, "Slot ring resonator and dispersion measurement on slot lines," *Electron. Lett.*, vol. 17. pp. 916–917, Nov. 1981.

[19] K. Kawano and H. Tomimuro, "Spectral domain analysis of an open slot ring resonator," *IEEE Trans. Microwave Theory Tech.*, vol. MTT-30, pp. 1184–1187, Aug. 1982.

[20] J. M. McCormic and M. G. Salvadori, *Numerical Methods in FORTRAN*. Englewood Cliffs, NJ: Prentice-Hall, 1964.

Kenji Kawano was born in Kitakyushu, Japan, on June 18, 1951. He received the B.S. and M.S. degrees in physics and applied physics from the Kyushu University, Fukuoka, Japan, in 1977 and 1979, respectively.

He joined the Musashino Electrical Communication Laboratory, Nippon Telegraph and Telephone (NTT) Public Corporation, Tokyo, Japan, in 1979, and has been engaged in the research of microwave integrated circuits. Recently, his major efforts have been directed towards the research and development for a laser diode to a single-mode fiber coupler.

Mr. Kenji Kawano is a member of the Institute of Electronics and Communication Engineers of Japan.